MIXED CONVECTION HEAT TRANSFER PAST IN-LINE SQUARE CYLINDERS IN A VERTICAL DUCT

by

Dipankar CHATTERJEE [a*] ***and Mohammad RAJA*** [b]

[a] Simulation & Modeling Laboratory, Central Mechanical Engineering Research Institute (Council of Scientific & Industrial Research), Durgapur, India
[b] Department of Mechanical Engineering, National Institute of Technology, Durgapur, India

Original scientific paper
DOI: 10.2298/TSCI101004199C

The mixed convection heat transfer around five in-line isothermal square cylinders periodically arranged within a vertical duct is numerically investigated in this paper. Spacing between two cylinders is fixed at one width of the cylinder dimension and the flow confinement of various degrees are studied for the blockage ratios of 0%, 10%, 25%, and 50%. The buoyancy aided/opposed convection is examined for the Richardson number ranges from –1 to +1 with a fixed Prandtl number 0.7 and Reynolds number 100. The transient numerical simulation for this 2-D, incompressible, laminar flow, and heat transfer problem is carried out by a finite volume based commercial computational fluid dynamics package FLUENT™. The representative streamlines and isotherm patterns are presented to interpret the flow and thermal transport visualization. Additionally, the time and surface average skin friction coefficient, drag, and lift coefficients as well as the time and surface average Nusselt number for representative cylinders are determined to elucidate the effects of Reynolds number and Richardson number on the flow and heat transfer phenomena.

Key words: *square cylinders, vertical channel, fluid flow, heat transfer, buoyancy aided/opposed convection, numerical simulation, low Reynolds number*

Introduction

Analysis of fluid flow and heat transfer behind multiple bluff obstacles such as circular/square cylinders at low Reynolds numbers (Re) has received considerable attention in view of practical engineering applications in heat exchangers, solar extraction systems, cooling towers, oil and gas pipelines, electronic cooling, *etc*. When flow passes over multiple bodies, wakes form and a complex flow structure originates as a consequence of the mutual interactions among them. Accordingly, the flow structure obtained behind multiple bluff bodies is significantly different from that obtained behind a single obstacle. Furthermore, the wake interactions strongly depend on the configuration and the spacing of the bodies to the incoming flow as well as on the geometrical shapes (for example circular or square cross sections) of the bodies. Consequently, the in-line, staggered or tandem arrangements of the obstacles offer different flow patterns. It should be mentioned that these arrangements of the obstacles are often followed in compact heat exchangers. Again, the flow patterns and the wake structures for the case of flow over square cylinders are significantly different from that over circular cylinders because of the fact that un-

* Corresponding author; e-mail: d_chatterjee@cmeri.res.in

like the circular cylinders the square cylinders tend to fix the separation point, causing differences in the critical regimes. Furthermore, the separation mechanisms depending on the shedding frequencies and the aerodynamic forces also differ significantly for these two geometries.

The flow even becomes more complicated when the wakes are further influenced by heat transfer. It should be recognized that for low to moderate Re flows, the buoyancy effect can significantly complicate the flow field, thereby affecting heat transfer characteristics. When the flow velocity is not very high but the temperature difference between the body and the fluid is significantly high, the heat transfer behavior is strongly influenced by thermal buoyancy. The thermal buoyancy plays a role of paramount importance on estimating the wake behavior since the wake structure is perturbed due to the superimposed thermal buoyancy resulting in hydrodynamic instabilities even at small Re. The buoyancy parameter, popularly known as the Richardson number (with Gr being the Grashof number) $Ri = Gr/Re^2$, provides a measure of the strength of free convection over the forced convection. The flow and thermal fields are completely dominated by free convection when Ri is sufficiently high ($Ri \gg 1$). Forced convection characterizes the transport phenomena for ($Ri \ll 1$) and both free and forced convections (*i. e.*, mixed convection) are equally important for $Ri \approx 1$. Buoyancy forces usually enhance the surface heat transfer rate when they aid the forced flow, whereas they impede the same when they oppose the forced flow. For the aiding case (flow past a heated body) the forced flow is in the same direction as the buoyancy force, whereas for the opposing case (flow past a cooled body), it is in the opposite direction.

Studies involving flow and heat transfer over a single or multiple bluff bodies (especially cylinders with circular or square cross sections) have been a subject of intense research in the past. Accordingly, a huge amount of pertinent experimental and numerical works are available in the literatures which are not explicitly mentioned here for the sake of brevity. In general, it is observed from a detailed survey that the studies related to the buoyancy aided/opposed flow and heat transfer over multiple cylinders, especially with the square cross section are less frequent in the literature compared to the studies involving the circular cylinders. In the context of laminar mixed convection heat transfer around horizontal cylinders in a vertical channel, Oosthuizen and Madan [1] studied experimentally the unsteady mixed convection for the range Re = 100-300. Merkin [2] reported that heating the circular cylinder delays separation and finally, the boundary layer does not separate at all. Jain and Lohar [3] found an increase in shedding frequency with a corresponding increase in the cylinder temperature. Farouk and Guceri [4] investigated numerically the laminar natural and mixed convection heat transfer around a heated circular cylinder placed within adiabatic channel walls. They also studied the effects of varying the ratio of width across the walls to cylinder diameter in the steady flow regime. Badr [5, 6] studied the laminar combined convection heat transfer from an isothermal horizontal circular cylinder for the two cases when the forced flow is directed either vertically upward (parallel flow) or vertically downward (contra flow) through the solution of the full vorticity transport equation together with the stream function and energy equations. The buoyancy-aided ($0 \le Ri \le 4$) steady convection heat transfer at low Re (= 20, 40, and 60) from a horizontal circular cylinder situated in a vertical adiabatic duct has been studied numerically by Ho *et al*. [7] for the blockage ratio parameter $B = 0$, 0.1667, 0.25, and 0.5. They observed a significant enhancement of the pure forced convection heat transfer due to the blockage effect as a result of placing the horizontal cylinder in the vertical duct. Chang and Sa [8] investigated the phenomenon of vortex shedding from a heated/cooled circular cylinder in the mixed convection regime and predicted the degeneration of purely periodic flows into a steady vortex pattern at a critical Ri of 0.15. Lacroix and Carrier [9] presented a numerical study of mixed convection heat transfer around two vertically separated horizontal cylinders within confining adiabatic walls. They investigated the effect of the cyl-

inder spacing, the distance between the plates, and Ri on the flow and heat transfer. Nakabe *et al*. [10] studied the effect of buoyancy on the channel-confined flow across a heated/cooled circular cylinder with a parabolic inlet velocity profile, by a finite difference method. The aiding, opposing and cross buoyancy cases were considered at Re = 80 and 120 for $-1 \le Ri \le 1.6$ and B = 0.15 and 0.3. The authors found three main results: first, at constant Re, the value of Ri at which the vortex shedding degenerates decreases with increasing blockage ratio; second, at constant blockage ratio, the value of Ri at which vortex shedding degenerates increases with Re; and third, at constant Ri, the value of Re at which vortex shedding starts goes on increasing with the increasing blockage ratio. The mixed convection heat transfer over an in-line bundle of cylinders was numerically studied by Gowda *et al*. [11, 12] for the range of Ri = –1 to +1. In another article, Gowda *et al*. [13] studied the heat transfer and fluid flow over a row of five in-line circular cylinders placed between two parallel plates. They investigated the problem for Re = 50 and 100 with a duct wall spacings of 1.5, 2, and 2.5 and Ri ranging from –5 to +5. It was established from their study that the buoyancy effect must be included during the forced convection analysis of flow over cylinders at low Re. By exploiting a finite element method, Singh *et al*. [14] determined the flow field and temperature distribution around a heated/cooled circular cylinder placed in an insulated vertical channel, with parabolic inlet velocity profile at Re = 100, $-1 \le Ri \le 1$, and B = 0.25. They observed that the vortex shedding stopped completely at a critical Ri of 0.15, below which the shedding of vortices into the stream was quite prominent. Patnaik *et al*. [15] studied numerically the influence of aiding and opposing buoyancy on the flow past an isolated circular cylinder. They observed that at low Re range (for, *e*. *g*., Re = 20-40), buoyancy opposing the flow could trigger vortex shedding. Saha [16] investigated the natural convection phenomena past a square cylinder placed centrally within a vertical parallel plate channel numerically using the MAC method. The flow was found unstable above the critical Gr ($Gr = 3 \cdot 10^4$). The drag coefficient was found to decrease while the Strouhal number (St) and surface-averaged Nu were seen to increase with Gr. Jue *et al*. [17] predicted numerically the heat transfer of transient mixed convective flow around three heated cylinders arranged in an isosceles right-angled triangle between two vertical parallel plates. The effect of buoyancy on the flow structure and heat transfer characteristics of an isolated square cylinder in upward cross flow was investigated numerically by Sharma and Eswaran [18] for Re = 100 and Pr = 0.7. Like the circular cylinder case, the degeneration of the Karman vortex street was also observed to occur at a critical Ri of 0.15 from their study for the more bluff square cylinder. In another article, Sharma and Eswaran [19] studied the effect of channel-confinement of various degrees ($B = 0.1$, 0.3, and 0.5) on the upward flow and heat transfer characteristics around a heated/cooled square cylinder by considering the effect of aiding/opposing buoyancy at $-1 \le Ri \le 1$, for Re = 100 and Pr = 0.7. They observed that with an increase in the blockage parameter, the minimum heating (critical Ri) required for the suppression of vortex shedding decreases up to a certain blockage parameter (= 0.3), but thereafter increases. Singh *et al*. [20] performed a comprehensive Schlieren-inter-ferometric study for the wakes behind heated circular and square cylinders placed in a vertical test cell. A detailed dynamical characteristic of vortical structures was reported in their study. The problem of the laminar upward mixed convection heat transfer for thermally developing air flow in the entrance region of a vertical circular cylinder under buoyancy effect and wall heat flux boundary condition has been numerically investigated by Hussein and Yasin [21] through an implicit finite difference method and the Gauss elimination technique. The investigation covers Re range from 400 to 1600 and the heat flux from 70 to 400 W/m^2. The results revealed that the secondary flow created by natural convection have a significant effect on the heat transfer process. The fluid flow and heat transfer characteristics around two isothermal square cylinders arranged in a tandem configuration with respect to the incoming flow within an insulated vertical channel at low Re range ($1 \le Re \le 30$) were estimated by Chatterjee [22] for a $B = 0.25$. The

buoyancy aided/opposed convection was examined for the Ri ranges from –1 to +1 with a fixed Pr of 0.7. Recently Gandikota *et al*. [23] studied the effect of thermal buoyancy on the upward flow and heat transfer characteristics around a heated/cooled circular cylinder for the range of parameters $-0.5 \le \mathrm{Ri} \le 0.5$, $50 \le \mathrm{Re} \le 150$, and $B = 0.02$ and 0.25.

From the critical evaluation of the pertinent available literature in the subject area, it is obvious that although there are some results for the mixed convection heat transfer analysis around circular cylinders placed confined within a vertical channel, the square counterpart is surprisingly less for the same configuration. Additionally, there is no reported work on the buoyancy aided/opposed mixed convection heat transfer over multiple square cylinders in a vertical configuration as frequently encountered in various chemical engineering applications. Accordingly, the aim of the present work is to numerically investigate the mixed convection heat transfer over five in-line row of heated/cooled cylinders with square cross section in a vertical 2-D channel. The study will be conducted for the $B = d/L = 00.1$, 0.25, and 0.5 at Re = 100 and Ri range of $-1 \le \mathrm{Ri} \le +1$ keeping the Pr constant.

Problem description

The geometry of the problem considered in this study along with the co-ordinate system used is shown schematically in fig. 1(a, b). Figures 1 (a) and (b), respectively depict the configurations for the channel confined (B = 10%, 25%, and 50%) and unconfined (B = 0%) cases. Five fixed identical 2-D square cylinders with sides d heated or cooled to a temperature T_w are arranged periodically and exposed to a uniform upward free stream with velocity v_∞ and temperature T_∞, as shown in fig. 1(a). Although the blockage is considered 0%, artificial confining boundaries are accepted around the flow with a blockage of 3.34% to make the problem computationally feasible. Two adiabatic vertical walls of finite length are placed at a distance of $L/2$ on either side of the center of the cylinders, fig. 1(b), for the channel confined flow cases. The upstream and downstream distances of the computational domain are chosen as H_U = 5 d and H_D = 34 d for the unconfined flow; and H_U = 8.5 d and H_D = 16.5 d for the channel confined flow. These values are chosen so as to reduce the effect of the inlet and outlet boundary conditions on the flow patterns in the vicinity of the cylinders and also they are consistent with the available literature [19].

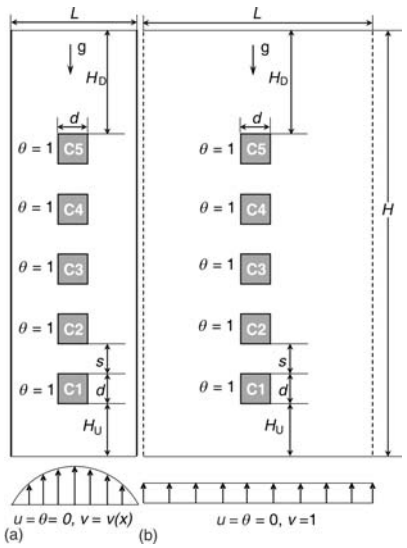

Figure 1. Schematic diagram of the computational domain, (a) channel confined and (b) unconfined flow

Governing equations

The dimensionless governing equations for this 2-D, laminar, incompressible flow with constant thermophysical properties along with Boussinesq approximation and negligible viscous dissipation can be expressed in the following conservative forms:

– *continuity*

$$\frac{\partial u}{\partial x} + \frac{\partial v}{\partial y} = 0 \tag{1}$$

– *momentum*

$$\frac{\partial u}{\partial t} + \frac{\partial (uu)}{\partial x} + \frac{\partial (uv)}{\partial y} = -\frac{\partial p}{\partial x} + \frac{1}{\mathrm{Re}}\left(\frac{\partial^2 u}{\partial x^2} + \frac{\partial^2 u}{\partial y^2}\right) \tag{2a}$$

$$\frac{\partial v}{\partial t}+\frac{\partial (uv)}{\partial x}+\frac{\partial (vv)}{\partial y}=-\frac{\partial p}{\partial x}+\frac{1}{\mathrm{Re}}\left(\frac{\partial^2 v}{\partial x^2}+\frac{\partial^2 v}{\partial y^2}\right)+\mathrm{Ri}\theta \tag{2b}$$

– *energy*

$$\frac{\partial \theta}{\partial t}+\frac{\partial (u\theta)}{\partial x}+\frac{\partial (v\theta)}{\partial y}=\frac{1}{\mathrm{Re}\,\mathrm{Pr}}\left(\frac{\partial^2 \theta}{\partial x^2}+\frac{\partial^2 \theta}{\partial y^2}\right) \tag{3}$$

where u, and v are the dimensionless velocity components along x- and y-directions of a Cartesian co-ordinate system, respectively, p and t the dimensionless pressure and time, and Re – the Re based on the cylinder dimension. The fluid properties are described by the density ρ, kinematic viscosity η, and thermal diffusivity α. The dimensionless variables are defined as:

$$u=\frac{\bar{u}}{v_\infty},\ v=\frac{\bar{v}}{v_\infty},\ x=\frac{\bar{x}}{d},\ y=\frac{\bar{y}}{d},\ p=\frac{\bar{p}}{\rho v_\infty^2},\ \theta=\frac{T-T_\infty}{T_\mathrm{w}-T_\infty},\ t=\frac{v_\infty \bar{t}}{d} \tag{4}$$

Boundary conditions

A parabolic velocity profile with the average velocity $v_{\mathrm{av}}=v_\infty$ is considered at the inlet for the channel confined flow (B = 10%, 25%, and 50%), whereas, a uniform free stream with velocity v_∞ is assumed for the unconfined flow (B = 0%). The vertical channel walls are assumed insulated and far-field boundary conditions are imposed on the artificial confining boundaries. The cylinder temperature T_w is governed by the magnitude of the Ri. A no-slip boundary condition is imposed on the cylinder surfaces and channel walls. The exit boundary is located sufficiently far downstream from the region of interest hence an outflow boundary condition is proposed at the outlet. Pressure boundary conditions are not explicitly required since the solver extrapolates the pressure from the interior. Mathematically, one can write the following:

– at the inlet

$$u=\theta=0,\ v=\begin{cases}1 & \text{for}\quad B=0\\ 1.5\left(1-\dfrac{x}{25}\right)^2 & \text{for}\quad B=0.10\\ 1.5\left(1-\dfrac{x}{4}\right)^2 & \text{for}\quad B=0.25\\ 1.5\,(1-x^2) & \text{for}\quad B=0.50\end{cases} \tag{5}$$

– at the outlet

$$\frac{\partial u}{\partial y}=\frac{\partial v}{\partial y}=\frac{\partial \theta}{\partial y}=0 \tag{6}$$

– at the vertical boundaries

$$\begin{aligned} &u=v=\frac{\partial \theta}{\partial x}=0 \quad \text{for}\quad B=0.1, 0.25, 0.5\\ &u=0,\ v=1,\ \theta=0 \quad \text{for}\quad B=0\end{aligned} \tag{7}$$

– at the cylinder surface:

$$u=v=0,\ \theta=1 \tag{8}$$

The flow is assumed to start impulsively from rest.

Solution procedure

The numerical simulation is performed by using the commercial CFD package *FLUENT* [24]. *FLUENT* uses a control volume based technique to solve the governing system of partial differential equations in a collocated grid system by constructing a set of discrete algebraic equations with conservative properties. The pressure based numerical scheme, which solves the discretized

governing equations sequentially, is selected. The laminar viscous model is selected to account for the low Re flow consideration. An implicit scheme is applied to obtain the discretized system of equations. The sequence updates the velocity field through the solution of the momentum equations using known values for pressure and velocity. Then, it solves a "Poisson-type" pressure correction equation obtained by combining the continuity and momentum equations. A second order upwind scheme is used for spatial discretization of the convective terms and a central difference scheme is used for the diffusive terms of the momentum and energy equations. Pressure-implicit with splitting of operators is selected as the pressure-velocity coupling scheme. The body-force-weighted pressure interpolation technique is used to interpolate the face pressure from the cell center values and the time discretization is carried out by a second order accurate fully implicit scheme. The conditions necessary to prevent numerical oscillations are determined from the Courant-Friedrichs-Lewy and the grid Fourier criteria. The final time step size is taken as the minimum of the two criteria mentioned above. Furthermore, the time step size is varied from 0.01 to 0.1 to determine an optimum value that results in less computational time, but produces sufficiently accurate results. A dimensionless time step size of 0.05 is finally used in the computation satisfying all of the above restrictions. The convergence criteria for the inner (time step) iterations are set as 10^{-6} for all the discretized governing equations.

A non-uniform grid distribution having a close clustering of grid points in the regions of large gradients and coarser grids in the regions of low gradients is used. Grids are generated using the grid generation package *GAMBIT* [24]. A comprehensive grid sensitivity study is carried out to select the most economical mesh sizes for the problem under consideration. As an example, three non-uniform mesh sizes (70×720, 80×750, and 90×780) are used to demonstrate the grid independence study for the case of $B = 0.5$, $\mathrm{Re} = 100$, and $\mathrm{Ri} = \pm 1$. The percentage change in the values of time average C_D and time and surface average Nu for the coarsest grid (70×720) with respect to the finest grid (90×780) are found to be 1.8 % and 0.6 %, respectively, while the same for the final two sets of grids are only 0.3% and 0.2%. Accordingly, 80×750 mesh size is preferred keeping in view the accuracy of the results and computational convenience in the simulations. Similar grid independence study for the other two are also performed and the optimized grid sizes of 130×750, 260×750, and 330×770 are finally chosen for $B = 0.25$, 0.1, and 0.0334, respectively. All the computations are carried out in an Intel (R) Xeon (R) CPU E5530 @ 2.40 GHz Workstation computer.

Validation

An extensive validation is performed before solving the present problem. In this purpose, numerical simulation is carried out for a single heated/cooled square cylinder subjected to aiding/opposing buoyancy for $-1 \le \mathrm{Ri} \le 1$ and at $\mathrm{Re} = 100$ and $\mathrm{Pr} = 0.7$. The parameters considered for validation purpose are taken from Sharma and Eswaran [19]. Figure 2(a) shows a comparison of the variation of dimensionless recirculation length (L_r) with Ri computed by the present solver and that reported by Sharma and Eswaran [19]. The recirculation length is defined as the stream-wise distance from the top surface of the cylinder to the re-attachment point along the wake centerline. The recirculation length increases steadily in the negative Richardson regime for lower blockage ratio ($B = 0.1$) with a subsequent steep rise in the aiding buoyancy condition, whereas, it decreases first and then increases subsequently for higher blockage ratio ($B = 0.5$). The present results are seen to be in very good agreement with that of the Sharma and Eswaran [19].

The St is plotted in fig. 2(b) for the aiding/opposing buoyancy cases. It increases monotonically with increasing Ri at a constant blockage ratio before it suddenly becomes zero due to the breakdown of the Karman vortex street. Again the agreement is satisfactory with the available results in the literature.

Finally, the cylinder average Nu for two blockage ratios (B = 0.1 and 0.5) are plotted against the Ri in fig. 2(c) and a slightly increasing tendency of Nu with Ri is observed. Overall, the comparison shows excellent agreement with the available results.

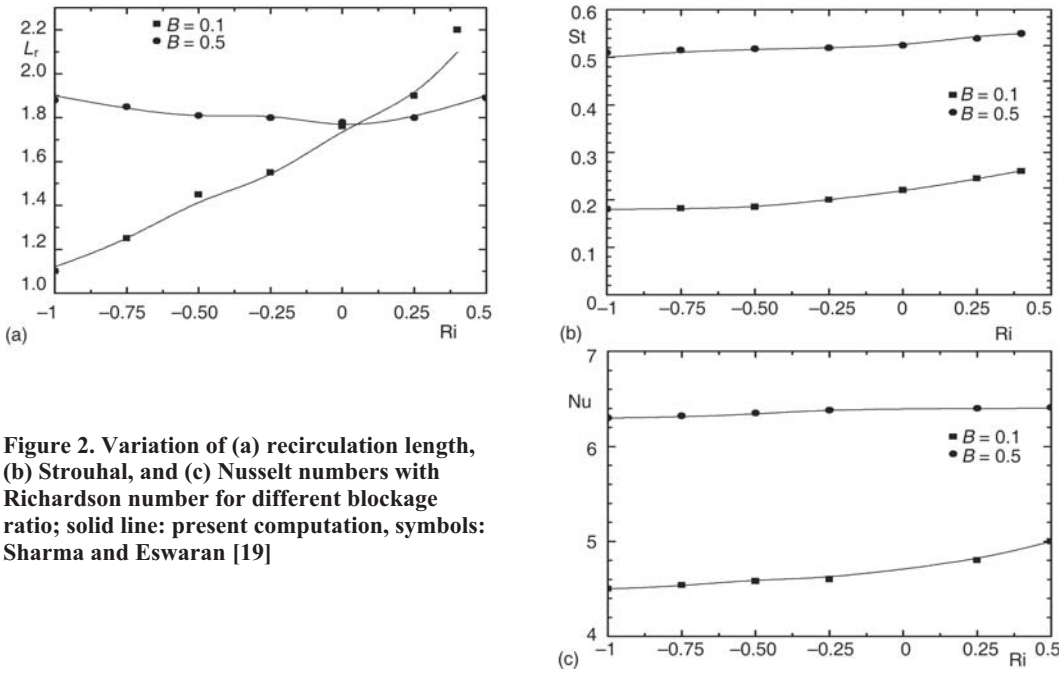

Figure 2. Variation of (a) recirculation length, (b) Strouhal, and (c) Nusselt numbers with Richardson number for different blockage ratio; solid line: present computation, symbols: Sharma and Eswaran [19]

Results and discussions

The present study aims to investigate the influence of aiding/opposing buoyancy on the overall flow patterns and the heat transfer characteristics for the upward flow past periodically arranged in-line cylinders of square cross-section at low Re. Furthermore, understanding of the variations of some important dimensionless global hydrodynamic and thermal parameters such as the skin friction coefficient, drag and lift coefficients and Nu under these conditions are also an important agenda. The flow is 2-D for the ranges of Re and Ri considered. With a dimensionless time step size of 0.05, the transient simulations for all the cases are carried out for 10000 time iterations (corresponding to a dimensionless time instant of 500) and results are obtained and presented for visual appreciation. The negative Ri signifies that the buoyancy force is in a direction opposite to that of the flow.

Representative streamlines and isotherm patterns (instantaneous) are shown for the cases of B = 0.5 and 0 at Re = 100 and for different Ri in figs. 3 and 4, respectively. For the case of pure forced convection (Ri = 0), an increase in B is associated with a corresponding increase in the strength of the recirculating flow between the cylinders. The wake region behind the fifth cylinder (from the bottom, C5) reduces owing to the blockage effect. In the negative Ri regimes (*i. e.* opposed buoyancy, Ri < 0), at the vicinity of the cylinder, the inertia force is opposed by the buoyancy as well as the viscous forces. As a consequence, there is an early separation that makes the wakes broader and a periodic vortex shedding can be observed. The streamline patterns are observed to have a wavering motion which increases with increased cooling of the cylinder. An almost chaotic motion is observed for the unconfined flow condition (B = 0) in the negative Ri.

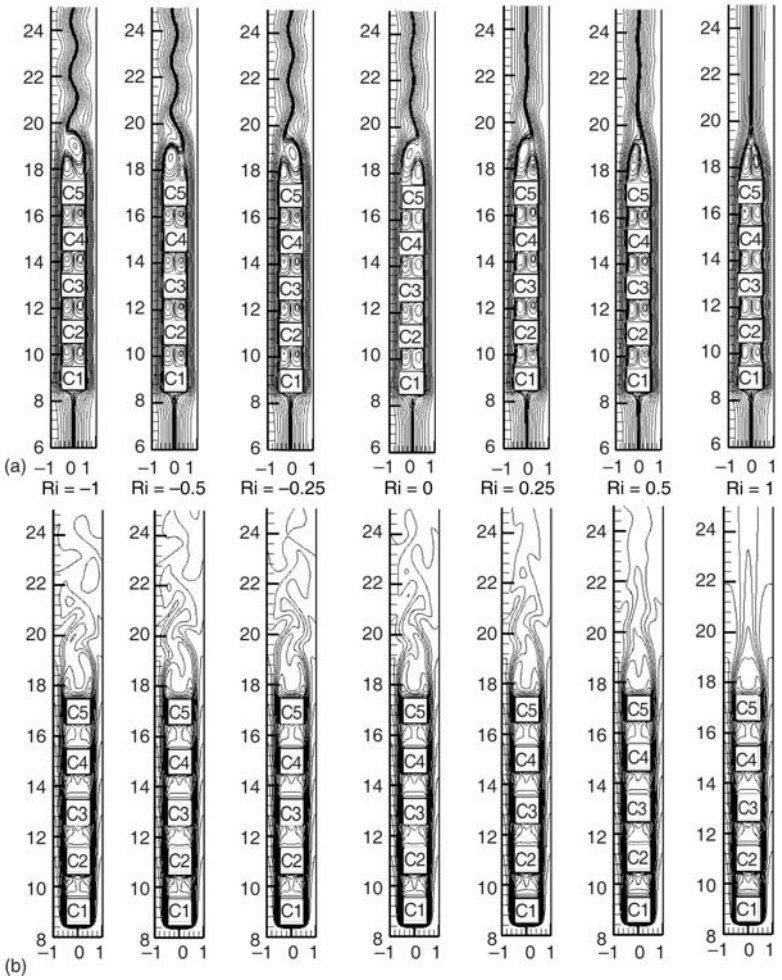

Figure 3. Instantaneous (a) streamlines and (b) isotherms for B = 0.5 and for different Richardson numbers

It should be mentioned that in the entire regime of negative Richardson numbers for all the cases the vortex shedding phenomena are quite prominent which is justified from the respective streamline plots. The shedding phenomena continue to characterize the flow even at Ri = 0 (*i. e.* for pure forced convection). However, the flow structure changes considerably for the positive Richardson regime (*i. e.*, for aiding buoyancy cases) and a critical value of Ri (Ri_{cr}) can be obtained where the vortex shedding is observed to stop completely. Under this aiding buoyancy condition, in the close proximity to the cylinder, the inertia force is added with the viscous force, resulting in a separation delay and the flow eventually becomes steady with a steady symmetric twin vortex behind the fifth cylinder. The isotherm profiles are the reflection of the physical phenomena observed from the analysis of the streamline patterns. The waviness of the isotherms downstream of the cylinder under the buoyancy opposed conditions is a clear indication of the periodic nature of the flow and thermal fields. This waviness can even be observed to persist like the vortex shedding phenomena up to the Ri_{cr}, above which the plume spread becomes narrower

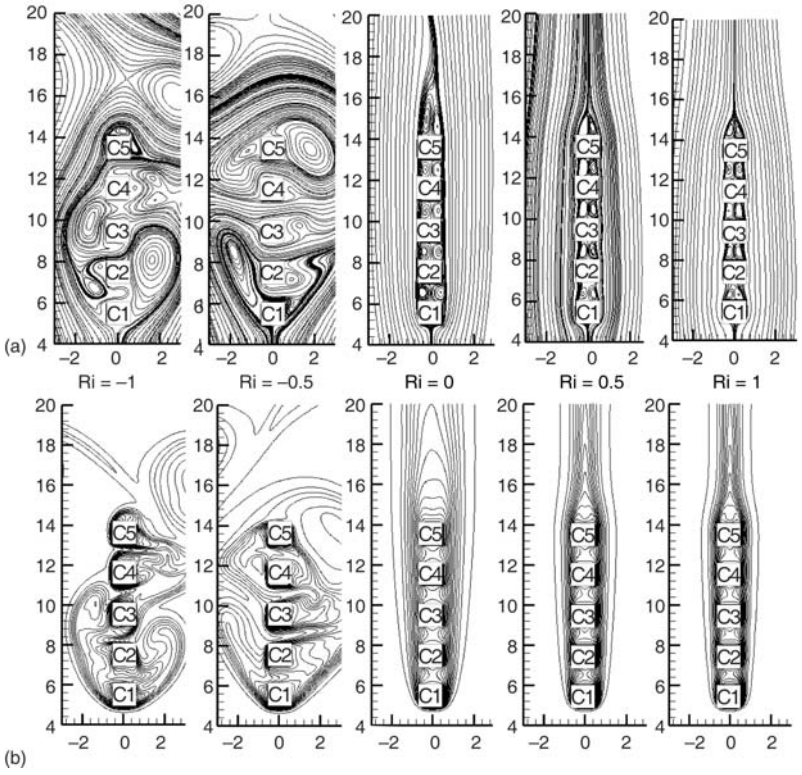

Figure 4. Instantaneous (a) streamlines and (b) isotherms for $B = 0$ and for different Richardson numbers

and the waviness subsequently disappears. The isotherm profiles show an almost symmetric nature (about the channel center line) like the streamlines for $Ri \geq Ri_{cr}$. It is to be noted that the isotherms are more crowded on the left, right and front surfaces of the bottom most cylinders (C1) for all cases and left and right, faces of other cylinders in the row indicating higher heat transfer rates on those surfaces as compared to the other surfaces of the cylinders.

To further establish the observations regarding the suppression of vortices at the Ri_{cr}, the dimensionless frequency of vortex shedding (St) is plotted against Ri for all the blockage parameters in fig. 5. The St, which characterizes the periodicity in a flow field, is defined as $St = f d/v_\infty$ where f is the vortex shedding frequency. The St is obtained from the fast Fourier transform of the transverse velocity component signal at the location 2.5 d downstream of the fifth cylinder (C5). The St is found to increase with increased heating of the cylinder above the fluid temperature (*i. e.* with increasing Ri). This

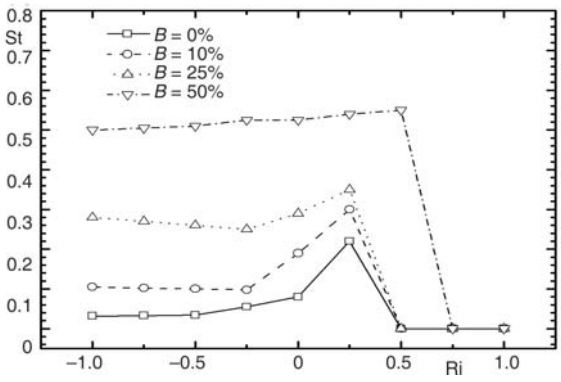

Figure 5. Strouhal *vs.* Richardson number for different blockage ratios

can be attributed by the fact that with increased heating of the cylinder, the fluid in the vicinity of the cylinder becomes lighter and hence the vortices detach from the cylinder. Upto the critical values of Ri, St increases, however, for Ri higher than the critical values, the frequency becomes suddenly zero, *i. e*. the shedding has stopped completely as a result of the breakdown of the Karman vortex street. It should be mentioned that for higher *B*, the shedding frequency is observed to be more compared to that for the lower one as a result of the effect of the confining walls which is consistent with earlier studies reported in the literature [25].

To understand the effect of thermal buoyancy on the global flow and heat transfer quantities, figs. 6-9 are plotted depicting the variation of time and surface average skin friction coefficient (C_f), drag (C_D), and lift (C_L) coefficients and time and surface average cylinder Nu with Ri for different *B*. The local skin friction coefficient is defined as:

$$C_f = \frac{\tau_w}{\frac{1}{2}\rho v_{av}^2} = \frac{2}{\mathrm{Re}}\frac{\partial v}{\partial x} + \frac{2}{\mathrm{Re}}\frac{\partial u}{\partial y} \tag{9}$$

where τ_w is the wall shear stress. The average skin friction coefficient is obtained by integrating the local value over the cylinder surface as:

$$\frac{2}{\mathrm{Re}}\int_0^1 \frac{\partial v}{\partial x}\mathrm{d}y + \frac{2}{\mathrm{Re}}\int_0^1 \frac{\partial u}{\partial y}\mathrm{d}x$$

Figures 6(a) and (b) shows the variation of time and surface average skin friction coefficient with Ri for $B = 0.5$ and 0, respectively. For the higher blockage ($B = 0.5$), the variation is almost linear and the average friction coefficient increases with increased heating of the cylinders, whereas a local minimum at Ri = 0 can be observed for the unconfined flow situation ($B = 0$). It is further to be noted that the average friction coefficient for the fifth cylinder (C5) is higher than that for the other cylinders and higher the blockage ratio more is the friction coefficient.

The drag and lift coefficients, C_D and C_L, respectively, on the cylinders include the pressure and viscous components and can be obtained as:

$$C_D = 2\int_0^1 p\mathrm{d}x + \frac{2}{\mathrm{Re}}\int_0^1 \frac{\partial v}{\partial x}\mathrm{d}y, \quad C_L = 2\int_0^1 p\mathrm{d}y + \frac{2}{\mathrm{Re}}\int_0^1 \frac{\partial u}{\partial y}\mathrm{d}x \tag{10}$$

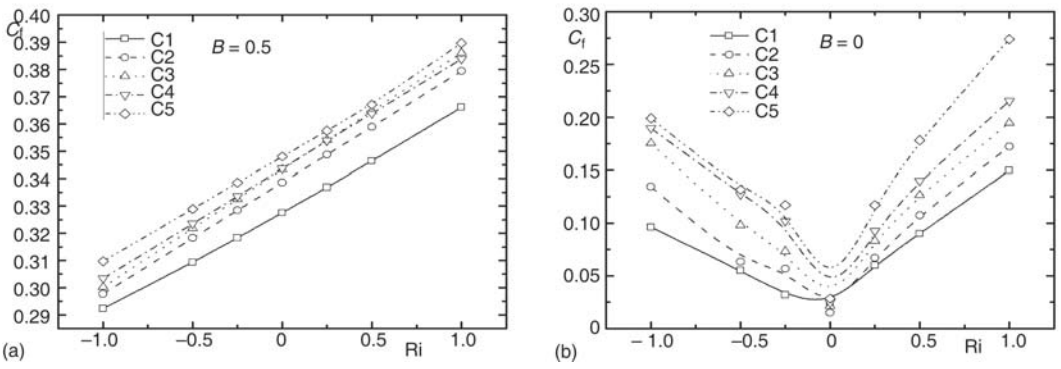

Figure 6. Variation of time and surface average skin friction coefficient with Richardson number at (a) $B = 0.5$ and (b) $B = 0$

The variations of C_D and C_L with Ri for all the cylinders are shown in figs. 7 and 8, respectively, at $B = 0.5$ and 0. For higher blockage ($B = 0.5$) the drag remains almost constant, whereas, at lower blockage ($B = 0$) there is a local minimum at Ri = 0. The drag coefficient for the first cylinder (C1) is always higher than the corresponding values of the other cylinders. The lift coefficients for various blockage ratios are found almost invariant with Ri. Since the lift force for the present case is experienced along the transverse direction, the effect of thermal buoyancy will not come into the picture. It is once again observed from figs. 9(a) and (b) that C_L is more for the unconfined flow situation than channel confined flows.

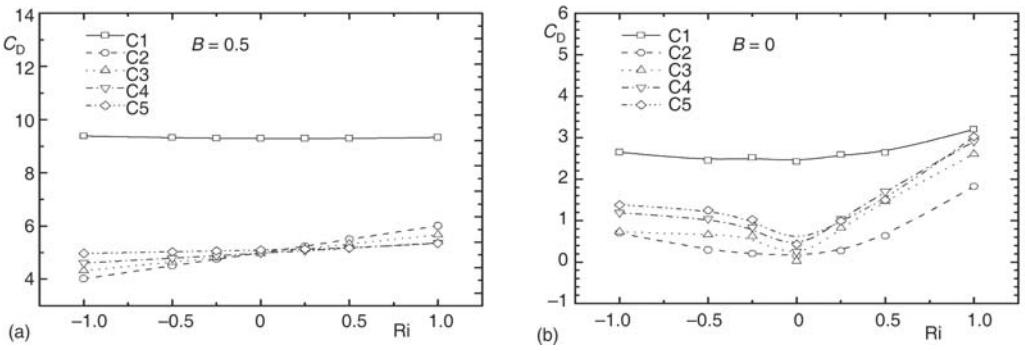

Figure 7. Variation of mean drag coefficient with Richardson number at (a) $B = 0.5$ and (b) $B = 0$

The heat transfer between the cylinders and the surrounding fluid is calculated by the Nu. The local Nu based on the cylinder dimension is given by:

$$\mathrm{Nu} = \frac{hd}{k} = -\frac{\partial\theta}{\partial n} \tag{11}$$

where h is the local heat transfer coefficient, k – the thermal conductivity of the fluid, and n – the direction normal to the cylinder surface. Surface average heat transfer at each face of the cylinders is obtained by integrating the local Nusselt number along the cylinder face. The time average Nu is computed by integrating the local value over a large time period. The average Nu as depicted in figs. 9(a) and (b) is almost invariant with Ri at higher blockage, whereas a local minima is observed close to Ri = 0 for unconfined case. The first cylinder (C1) is always having higher Nu compared to the other cylinders indicating higher heat transfer from the first cylinder.

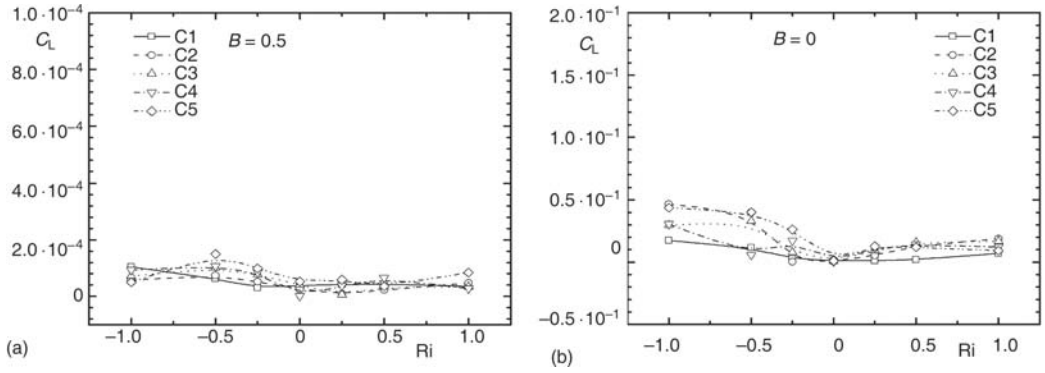

Figure 8. Variation of mean lift coefficient with Richardson number at (a) $B = 0.5$ and (b) $B = 0$

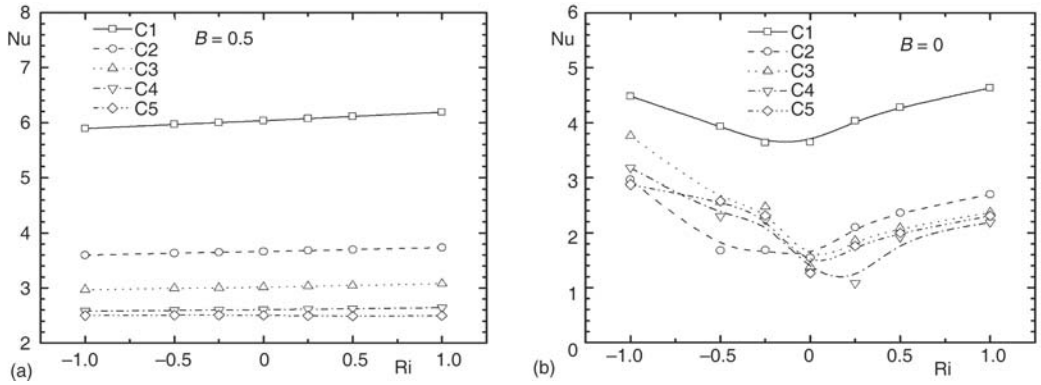

Figure 9. Variation of time and surface average cylinder Nusselt number with Richardson number at (a) $B = 0.5$ and (b) $B = 0$

This is because the temperature difference between the cylinder wall and the fluid is higher for C1 and consequently, higher heat transfer occurs in case of first cylinder. The variation of time and surface average cylinder Nu with blockage ratio for the first and fifth cylinders in the row (C1 and C5) is shown in figs. 10(a) and (b) at Ri = 1 and –1. The average Nu increases with blockage ratio for C1 as a result of the heat transfer contribution from the confining walls as evident form fig. 10(a). However, for the fifth cylinder, the average Nu decreases with blockage for the opposed buoyancy condition as shown in fig. 10(b).

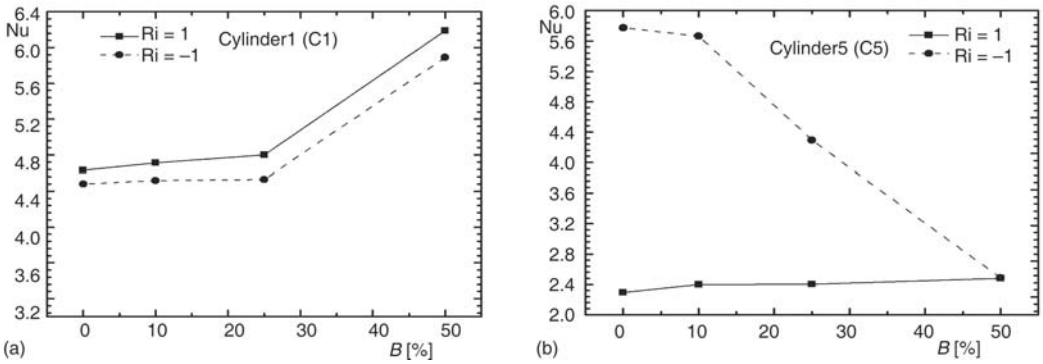

Figure 10. Variation of time and surface average cylinder Nusselt number with blockage ratio for the (a) first cylinder (C1) and (b) fifth cylinder (C5) at Ri = 1 and –1

In the negative Richardson regimes (*i. e.* opposed buoyancy, Ri < 0), at the vicinity of the cylinder, the inertia force is opposed by the buoyancy as well as the viscous forces. However, for the positive Richardson regime (*i. e.*, for aiding buoyancy cases, Ri > 0), in the close proximity to the cylinder, the inertia force is added with the viscous force, resulting in a separation delay. As a consequence, the drag, lift and the skin friction coefficient decrease in the negative Richardson regime (Ri < 0), reach a minimum value at Ri = 0 and then again increase in the positive Richardson regime (Ri > 0). This phenomena is observed for the unconfined flow (B = 0), however for higher blockage (B = 0.5) due to the stabilizing effect of the wall the effect of natural convection on the shedding phenomena is diminished. For the same reasoning the heat transfer rate (Nu) is also observed to show similar variation.

Conclusions

Fluid flow and heat transfer from five in-line heated/cooled square cylinders fixed within a vertical confining space (B = 0, 0.1, 0.25, and 0.5) in the 2-D steady laminar flow regimes are investigated in this work. The effects of aiding/opposing buoyancy on the flow and heat transfer are extensively studied for the Ri range of $-1 \le \mathrm{Ri} \le 1$and at Re = 100, keeping a fixed Prandtl value (Pr = 0.7). The most interesting observation from the study is the suppression of Karman vortices at a critical value of the Ri, below which the vortices shed in a periodic manner. The periodic vortex shedding are commonly observed for the opposed buoyancy (Ri < 0) cases, whereas the vortex shedding phenomena are stopped mostly for the aided buoyancy cases. It is also observed that for higher blockage ratio, the shedding frequency is more compared to that for the lower one as a result of the effect of the confining walls. The other overall observations regarding the characteristic features of some important global flow and heat transfer quantities subjected to the aiding/opposing buoyancy and channel confinement are given as:

- the average friction coefficient increases with increased heating of the cylinders for higher blockage, whereas a local minimum at Ri = 0 can be observed for the unconfined flow,
- for higher blockage (B = 0.5) the drag remains almost constant, whereas, at lower blockage (B = 0) there is a local minimum at Ri = 0,
- the lift coefficients for various blockage ratios are found almost invariant with Ri,
- the average Nu is almost invariant with Ri at higher blockage, whereas a local minima is observed close to Ri = 0 for unconfined case, and
- the average Nu increases with the blockage ratio.

The following general thermohydrodynamic features for the cylinders can also be observed:

- the time and surface average skin friction coefficient is more for the fifth cylinder (C5) in comparison to other cylinders in the row,
- the mean drag is found to be more for the first cylinder (C1), and
- the first cylinder (C1) is always having higher Nu compared to the other cylinders indicating higher heat transfer from the first cylinder.

Nomenclature

B – blockage ratio, (= d/L)
C_D – drag coefficient, [–]
C_f – skin friction coefficient, [–]
C_L – lift coefficient, [–]
C1–C5 – cylinder, [–]
d – cylinder size, [m]
f – frequency, [Hz]
g – acceleration due to gravity, [ms^{-2}]
Gr – Grashof number, (= $g\beta(T_w - T_\infty)d^3/\eta^2$)
H – height of computational domain, [m]
h – local heat transfer coefficient, [Wm^{-2}K^{-1}]
k – thermal conductivity of fluid, [Wm^{-1}K^{-1}]
L – width of computational domain, [m]
L_r – dimensionless recirculation length, (= L_r/d)
Nu – local Nusselt number, (= hd/k)
n – normal direction, [–]
Pr – Prandtl number, (= η/α)
p – dimensionless pressure, (= $\overline{p}/\rho u_\infty^2$)
Re – Reynolds number, (= $u_\infty d/\eta$)
Ri – Richardson number, (= Gr/Re^2)
St – Strouhal number, (= fd/v_∞)
s – spacing between cylinders, [m]
T – temperature, [K]
T_w – cylinder temperature, [K]
T_∞ – free stream temperature, [K]
t – dimensionless time, (= $u_\infty t/d$)
v_∞ – free stream velocity, [ms^{-1}]
u – dimensionless axial velocity, (= $\overline{u}/v_\infty$)
v – dimensionless normal velocity, (= $\overline{v}/v_\infty$)
x – dimensionless axial co-ordinate, (= $\overline{x}/d$)
y – dimensionless normal co-ordinate, (= $\overline{y}/d$)

Greek symbols

α – thermal diffusivity of the fluid, [m^{2}s^{-1}]
β – coefficient of volume expansion, [K^{-1}]
η – kinematic viscosity of fluid, [m^{2}s^{-1}]
θ – dimensionless temperature, [=$(T - T_\infty)/(T_w - T_\infty)$]
ρ – density of the fluid, [kgm^{-3}]
τ_w – wall shear stress, [Nm^{-2}]

Subscripts

av – average
cr – critical
∞ – free stream

Superscripts

$^-$ – dimensional quantity

References

[1] Oosthuizen, P. H., Madan, S., The Effect of Flow Direction on Combined Convective Heat Transfer from Cylinders to Air, *Journal of Heat Transfer, 93* (1971), 2, pp. 240-242
[2] Merkin, J. H., Mixed Convection from a Horizontal Circular Cylinder, *International Journal of Heat and Mass Transfer, 20* (1977), 1, pp. 73-77
[3] Jain, P. C., Lohar, B. L., Unsteady Mixed Convection Heat Transfer from a Horizontal Circular Cylinder, *Transaction of ASME Journal of Heat Transfer, 101* (1979), 1, pp. 126-131
[4] Farouk, B., Guceri, S. I., Natural and Mixed Convection Heat Transfer around a Horizontal Cylinder Within Confining Walls, *Numerical Heat Transfer A, 5* (1982), 3, pp. 329-341
[5] Badr, H. M., Laminar Combined Convection from a Horizontal Cylinder-Parallel and Contra Flow Regime, *International Journal of Heat and Mass Transfer, 27* (1984), 1, pp. 15-27
[6] Badr, H. M., On the Effect of Flow Direction on Mixed Convection from a Horizontal Cylinder, *International Journal of Numerical Methods in Fluids, 5* (1985), 1, pp. 1-12
[7] Ho, C. J., *et al*., Analysis of Buoyancy-Aided Convection Heat Transfer from a Horizontal Cylinder in a Vertical Duct at Low Reynolds Number, *Heat and Mass Transfer, 25* (1990), 6, pp. 337-343
[8] Chang, K. S., Sa, J. Y., The Effect of Buoyancy on Vortex Shedding in the Near Wake of a Circular Cylinder, *Journal of Fluid Mechanics, 220* (1990), pp. 253-266
[9] Lacroix, M., Carrier, R., Mixed Convection Heat Transfer from Vertically Separated Horizontal Cylinders Within Confining Walls, *Numerical Heat Transfer A, 27* (1995), 4, pp. 487-498
[10] Nakabe, K., *et al*., Heat Transfer from a Heated Cylinder in a Flow between Parallel Plates in a Free-Forced Combined Convection Regime, *Proceedings*, 9th International Symposium on Transport Phenomena in Thermal Fluids Engineering, Singapore, 1996, pp. 651-656
[11] Krishne Gowda, Y. T., *et al*., Numerical Investigation of Mixed Convection Past in-Line Tube Bundles, *Heat and Mass Transfer, 31* (1996), 5, pp. 347-352
[12] Krishne Gowda, Y. T., *et al*., Buoyancy Effect on Flow and Teat Transfer Past in-Line Tube Bundles, *Proceedings*, ISHMT and ASME Heat and Mass Transfer Conference, Surathkal, India, 1995, pp.763-768
[13] Krishne Gowda, Y. T., *et al*., Mixed Convection Heat Transfer Past In-Line Cylinders in a Vertical Duct, *Numerical Heat Transfer A, 31* (1997), 5, pp. 551-562
[14] Singh, S., *et al*., Effect of Thermal Buoyancy on the Flow through a Vertical Channel with a Built-in Circular Cylinder, *Numerical Heat Transfer A, 34* (1998), 7, pp. 769-789
[15] Patnaik, B. S. V., *et al*., Numerical Simulation of Vortex Shedding Past a Circular Cylinder under the Influence of Buoyancy, *International Journal of Heat and Mass Transfer, 42* (1999), 8, pp. 3495-3507
[16] Saha, A. K., Unsteady Free Convection in a Vertical Channel with a Built-in Heated Square Cylinder, *Numerical Heat Transfer A, 38* (2000), 8, pp. 795-818
[17] Jue, T. C., *et al*., Heat Transfer Predictions around Three Heated Cylinders between two Parallel Plates, *Numerical Heat Transfer A, 40* (2001), 7, pp. 715-733
[18] Sharma, A., Eswaran, V., Effect of Aiding and Opposing Buoyancy on the Heat and Fluid Flow across a Square Cylinder at Re = 100, *Numerical Heat Transfer A, 45* (2004), 6, pp. 601-624
[19] Sharma, A., Eswaran, V., Effect of Channel-Confinement and Aiding/Opposing Buoyancy on the Two-Dimensional Laminar Flow and Heat Transfer across a Square Cylinder, *International Journal of Heat and Mass Transfer, 48* (2005), 25-26, pp. 5310-5322
[20] Singh, P. S. K., *et al*., Effect of Buoyancy on the Wakes of Circular and Square Cylinders: A Schlieren-Interferometric Study, *Experiments in Fluids, 43* (2007), 1, pp. 101-123
[21] Hussein, A. M., Yasin, K. S., Numerical Study of Combined Convection Heat Transfer for Thermally Developing upward Flow in a Vertical Cylinder, *Thermal Science, 12* (2008), 2, pp. 89-102
[22] Chatterjee, D., Mixed Convection Heat Transfer from Tandem Square Cylinders in a Vertical Channel at Low Reynolds Numbers, *Numerical Heat Transfer A, 58* (2010), pp. 740-755
[23] Gurunath, G., *et al*., Effect of Aiding/Opposing Buoyancy on Two-Dimensional Laminar Flow and Heat Transfer across a Circular Cylinder, *Numerical Heat Transfer A, 58* (2010), 5, pp. 385-402
[24] ***, FLUENT 6.0 User's Guide, Vol. 5, Fluent Inc., Lebanon, 2001
[25] Mukhopadhyay, A., *et al*., Numerical Investigation of Confined Wakes Behind a Square Cylinder in a Channel, *International Journal for Numerical Methods in Fluids, 14* (1992), 12, pp. 1473-1484

Paper submitted: April 10, 2010
Paper revised: February 8, 2012
Paper accepted: November 24, 2012